Detailed Heat Transfer Measurements of Various Rib Turbulator Shapes at Very High Reynolds Numbers Using Steady-state Liquid Crystal Thermography

Mingyang Zhang

Thesis submitted to the faculty of the
Virginia Polytechnic Institute and State University
in partial fulfillment of the requirements for the degree of

Master of Science
In
Mechanical Engineering

Srinath V. Ekkad Chair
Ranga Pitchumani
Rui Qiao

December 18, 2017
Blacksburg, VA

Keywords: High Reynolds number; rib turbulators; thermal hydraulic performance

Detailed Heat Transfer Measurements of Various Rib Turbulator Shapes at Very High Reynolds Numbers Using Steady-state Liquid Crystal Thermography

Mingyang Zhang

ABSTRACT

In order to protect gas turbine blades from hot gases exiting the combustor, several intricate external and internal cooling concepts are employed. High pressure stage gas turbine blades feature serpentine passages where rib turbulators are installed to enhance heat transfer between the relatively colder air bled off from the compressor and the hot internal walls. Most of the prior studies have been restricted to Reynolds number of 90000 and several studies have been carried out to determine geometrically optimized parameters for achieving high levels of heat transfer in this range of Reynolds number. However, for land-based power generation gas turbines, the Reynolds numbers are significantly high and vary between 10^5 and 10^6. Present study is targeted towards these high Reynolds numbers where traditional rib turbulator shapes and prescribed optimum geometrical parameters have been investigated experimentally. A steady-state liquid crystal thermography technique is employed for measurement of detailed heat transfer coefficient. Five different rib configurations, viz., 45 deg., V-shaped, inverse V-shaped, W-shaped and M-shaped have been investigated for Reynolds numbers ranging from 150,000 to 400,000. The ribs were installed on two opposite walls of a straight duct with aspect ratio of unity. For very high Reynolds numbers, the heat transfer enhancement levels for different rib shapes varied between 1.3 and 1.7 and the thermal hydraulic performance was found to be less than unity.

Detailed Heat Transfer Measurements of Various Rib Turbulator Shapes at Very High Reynolds Numbers Using Steady-state Liquid Crystal Thermography

Mingyang Zhang

GENERAL AUDIENCE ABSTRACT

Gas turbine blades operate in hot gases exiting from combustor. The temperature of the hot gas is much higher than the melting point of blades material. To protect gas turbine blades several intricate external and internal cooling technique have been applied. Inside the blades, impingement cooling, rib turbulators cooling and pin fins cooling technique are applied in the leading edge, central body and trailing edge, respectively. At the central body serpentine passage was manufactured where rib turbulators are installed to enhance heat transfer between the relatively colder air bled off from the compressor and the hot internal walls. This is attributed to the colder air's boundary layer is tripped by the rib turbulators enhance the flow turbulence. All the previous works are based on lower Reynolds number (under 90000) which always happens in aircraft gas turbine engine. In land based gas turbine the Reynolds numbers of cooling air are significantly high and vary between 10^5 and 10^6. Present study is targeted towards these high Reynolds numbers where traditional rib turbulator shapes and prescribed optimum geometrical parameters have been investigated experimentally. Five different rib configurations, viz., 45 deg., V-shaped, inverse V-shaped, W-shaped and M-shaped have been investigated for Reynolds numbers ranging from 150,000 to 400,000. For very high Reynolds numbers, the heat transfer enhancement levels for different rib shapes varied between 1.3 and 1.7 and the thermal hydraulic performance was found to be less than unity. It's a caution to turbine hot gas path designers, particularly for the cases where rib designs for aircrafts are used in land based power generationgas turbines

ACKNOWLEDGEMENTS

I would like to express my sincere gratitude to Dr. Srinath V. Ekkad for giving me the opportunity to work with him. His encouragements and valuable guidance have helped me to growth. He has been and will always inspires me to move forward.

I would like to thanks Dr. Prashant Singh and Dr. Jaideep Pandit for sharing their experience and helping for my experiment.

I would like to thanks for all of my wonderful friends. Yuqin Li, Ruihao Wang, Xin Jin, Yan Song and Ze Cao thanks for all of your support.

Also I would like to thanks my family, without the love and support and encouragement for my mom and dad all this would not be possible

Table of Contents

List of Figures

Detailed Heat Transfer Measurements of Various Rib Turbulator Shapes at Very High Reynolds Numbers Using Steady-state Liquid Crystal Thermography

Mingyang Zhang
Department of Mechanical Engineering,
Virginia Tech, Blacksburg, VA 24061

Prashant Singh
Department of Mechanical and Aerospace Engineering
North Caroline State University, Raleigh, NC

Srinath V. Ekkad
Department of Mechanical and Aerospace Engineering
North Caroline State University, Raleigh, NC

ABSTRACT

In order to protect gas turbine blades from hot gases exiting the combustor, several intricate external and internal cooling concepts are employed. High pressure stage gas turbine blades feature serpentine passages where rib turbulators are installed to enhance heat transfer between the relatively colder air bled off from the compressor and the hot internal walls. Most of the prior studies have been restricted to Reynolds number of 90000 and several studies have been carried out to determine geometrically optimized parameters for achieving high levels of heat transfer in this range of Reynolds number. However, for land-based power generation gas turbines, the Reynolds numbers are significantly high and vary between 10^5 and 10^6. Present study is targeted towards these high Reynolds numbers where traditional rib turbulator shapes and prescribed optimum geometrical parameters have been investigated experimentally. A steady-state liquid crystal thermography technique is employed for measurement of detailed heat transfer coefficient. Five different rib configurations, viz., 45 deg., V-shaped, inverse V-shaped, W-shaped and M-shaped have been investigated for Reynolds numbers ranging from 150,000 to 400,000. The ribs were installed on two opposite walls of a straight duct with aspect ratio of unity. For very high Reynolds numbers, the heat transfer enhancement levels for different rib

shapes varied between 1.3 and 1.7 and the thermal hydraulic performance was found to be less than unity.

INTRODUCTION

Higher turbine inlet temperatures are required for high turbine efficiency. Hot gas path turbine components are subjected to elevated heat loads from hot gases exiting the combustor section. To protect the hot gas path components from hot gases, sophisticated internal and external cooling concepts are employed in turbine airfoils. Relatively colder air bled off from the compressor section is routed through complicated internal cooling passages to cool the hot internal walls of turbine airfoils. However, the coolant bled from the compressor reduces the turbine efficiency. Hence, it is imperative to develop cooling concepts which have high heat transfer enhancement levels at relatively lower enhancement in pumping power. Considerable research has been carried out to develop internal cooling concepts which have high rates of heat transfer between the coolant and the blade internal walls.

Turbine airfoil internal cooling passages are equipped with rib turbulators for heat transfer enhancement. Han et al. [1] presented a detailed overview of the various geometric and flow parameters which influence ribbed channel heat transfer like rib spacing, their orientation, channel aspect ratio, rib shape etc. First few studies were focused on rib turbulators placed orthogonal to flow where heat transfer enhancement mechanism was due to flow reattachment leading to very thin turbulent boundary layer [2]. Heat transfer enhancement levels by rib turbulators underwent significant enhancement when ribs were placed at an angle of attack with bulk flow. The heat transfer enhancement in such configurations was due to increase in near-wall shear stress due to generation of secondary flows and increase in turbulent transport [3-6]. Different types of inclined ribs such as, crossed ribs, V-shape, inverted V-shape, broken V-shaped rib, M-shaped, W-shaped, criss-cross pattern formed by 45-deg angled ribs, rib channel with grooves, rib dimpled compound channels, etc. have been studied in [7-15].

Heat transfer coefficient measurement techniques include steady state copper blocks, transient liquid crystal and infrared thermography technique, steady-state liquid crystal thermography etc. Leiss [16], Han et al. [17] and Han [18] have used thin foil heater steady-state technique for surface heat transfer coefficient measurement. Fan and Metzger [19], Wagner et al. [20], and Han et al. [21] have all used copper plates and presented regional averaged measurements inside stationary and rotating internal cooling channels. Steady-state techniques

employing copper based heating blocks provide regionally averaged heat transfer coefficient. However, for detailed knowledge of local heat transfer coefficient, liquid crystal thermography is used. Ekkad and Han [22] were the first to present detailed Nusselt number distributions for a two-pass square channel using transient liquid crystal technique. Their study provided useful insight into the role of rib induced secondary flow on local heat transfer. Jenkins et al. [23] used transient liquid crystal technique to investigate the heat transfer distribution and pressure losses for a ribbed two- pass varying aspect ratio cooling channel with different divider wall-to-tip wall distance. Transient liquid crystal experiments provide useful insight into heat and fluid flow in complicated internal cooling ducts. These experiments are short duration and employ a low thermal conductivity material for the one-dimensional semi-infinite assumption. Liquid crystals can also be used in steady-state experiments as well. Tanda and Abram [24] carried out experiments using steady state liquid crystal thermography on 45-degree angled turbulators for Reynolds number ranging from 9000 to 35500, and reported heat transfer augmentation in the range of 2.7 to 1.8. Steady-state liquid crystal thermography technique was used by Tanda [25] to investigate the effects of pitch-to-height ratio of 45-degree ribs in a rectangular channel with aspect ratio of five.

Based on our literature survey, we found that several studies have been carried out in past to explore different rib shapes in terms of heat transfer enhancement and thermal hydraulic performance using different measurement techniques. However, most of these studies investigated heat transfer characteristics of rib roughened ducts upto Reynolds numbers of 90000, catering towards aircraft engines. Experimental study by Rallabandi et al. [26] investigated heat transfer and frictional characteristics of 45-degree angled rib turbulators for Reynolds numbers ranging from 30000 to 400000. This was the first study to push the rib roughened duct heat transfer database to such high Reynolds numbers. The authors employed steady-state copper bar heat transfer measurement technique and reported regionally averaged Nusselt number ratio (Nu/Nu_0).

Present study is focused on detailed measurement of heat transfer coefficient for different rib shapes at very high Reynolds numbers. The Reynolds numbers ranged from 150,000 to 400,000 and were chosen for land-based gas turbine engines. Detailed heat transfer coefficients were measured using steady-state liquid crystal thermography. Five different rib configurations, viz., 45-deg inline, M-shaped, W-shaped, V-shaped, inverted V-shape, have been investigated. The rib

turbulators were square in shape and the rib-height to channel-hydraulic-diameter ratio (e/d_h) was 0.1 and rib-pitch to rib-height ratio (p/e) was 10. The ribs were installed on two opposite walls of a straight duct with aspect ratio of unity. Heat transfer enhancement levels (Nu/Nu_0) and thermal hydraulic performance of different rib turbulator configurations have been reported and the heat transfer enhancement mechanism at high Reynolds numbers has been discussed.

EXPERIMENTAL SETUP

Figure 1 presents a schematic of the experimental setup. Laboratory ambient air was drawn into the test section via a pressure blower (The New York Blower Company, wheel type 1710 ALUM, static pressure 20.1 "H_2O). The blower was driven by a 20 HP electric motor and the motor was controlled by a fine tune variable frequency drive. The blower was connected to a contraction section which gradually converted the circular cross-section to a square cross-section. The square duct featured rib turbulators of different shapes. The duct was made out of plexiglass, which is a low thermal conductivity transparent material. The rib shapes were additively manufactured using ABS and had a thermal conductivity of $0.19\ W/mK$. Low thermal conductivity materials were used for assembling the test sections to minimize the heat loss during the forced convection experiments. Liquid crystal sheets were installed between the rib pitches for measurement of local wall temperatures. A wide band liquid crystal sheet (R30C5W) manufactured by LCR Hallcrest was used in the present study. The assembly of liquid crystal sheet is shown in Fig. 2.

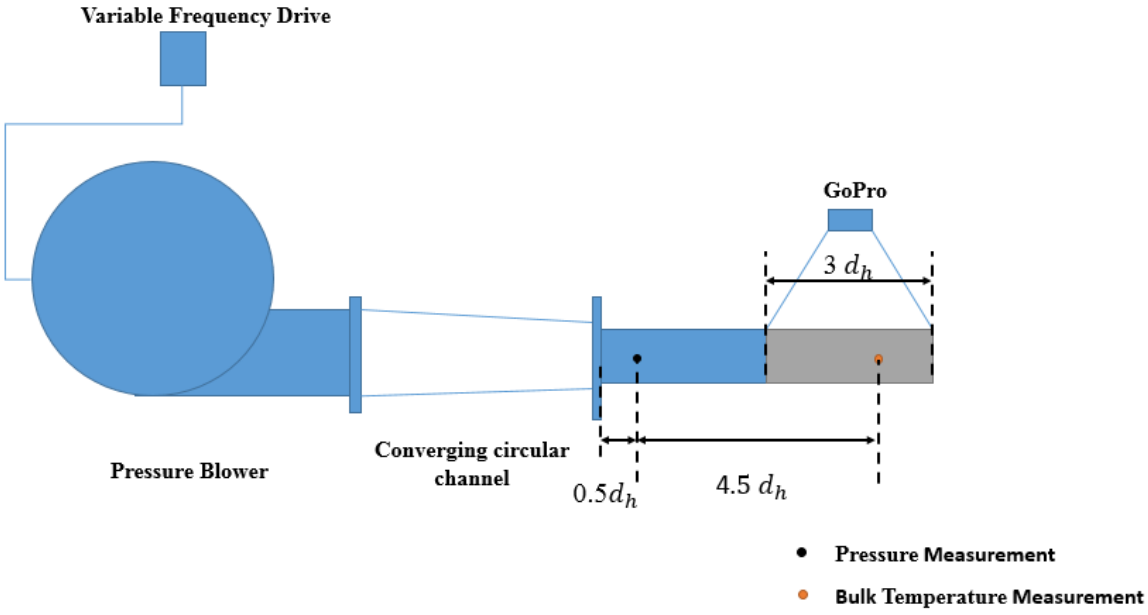

Fig. 1 Schematic of experimental setup

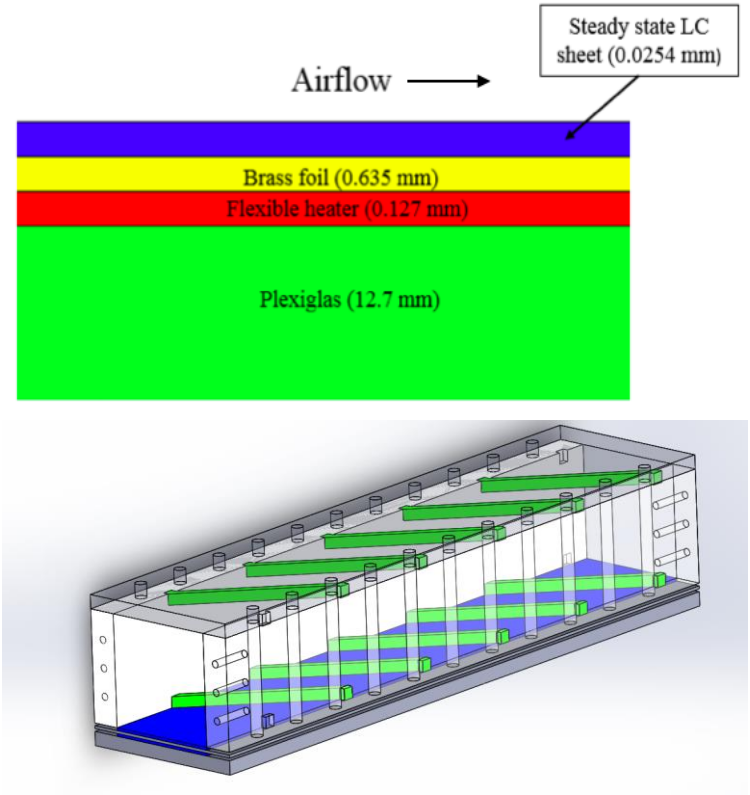

Fig. 2 Liquid crystal assembly (not drawn to scale), isometric view of the ribbed channel (blue color indicating TLC sheet)

Flexible heater of size 101.6 mm x 304.8 mm and thickness of 0.127 mm, manufactured by Omega Engineering (KH-412/10-p) was glued on top of plexiglass enclosure. The power to the heater was provided by a fine control variac (Circuit specialist: TDGC-0.5KM). The variac was capable of supplying voltage up to 130 volts at 60 Hz. The voltage and resistance across the heater was measured by a highly accurate Agilent digital Multimeter (34401A). To uniformly distribute the heat flux across the channel span, a thin brass sheet of thickness 0.635 mm was secured on top of the flexible heater. Liquid crystal sheets of thickness 0.0254 mm were then glued on top of the brass foil. Different layers of heater, brass foil and liquid crystal sheets were compressed via. uniformly spaced through bolts on the side walls. The side walls also had provisions for accommodating the extreme ends of ribs. Hence, compression force on the side walls through bolts also helped disburse the compression force along the ribs in the channel span. It was made sure that different layers of the heat transfer test section were in good contact with each other.

The liquid crystal color change was illuminated by diffused cool lighting kept at an angle of 45-degrees with respect to bulk flow direction. It was made sure that there were no reflections from the side walls and top wall on liquid crystal color change at the bottom end of the test section. The test section was covered with black cover to block any ambient lighting. The liquid crystal color change was viewed from the opposite end through the transparent plexiglass. Hence, the data on the ribs could not be obtained due to optical blockage. The color change was captured by a GoPro Hero 4 camera at a spatial resolution of 1080 x 1920. The camera field of view was adjusted such that only the region of interest was captured.

Description of test configurations and experimental conditions

Five different rib turbulator shapes were tested in the present study. Different rib configurations have been shown in Fig. 3. The channel hydraulic diameter was ten times the rib height. Hence the channel blockage due to ribs was 20% since ribs were installed on opposite walls of the channel. Heat transfer coefficients were measured on only one wall given the symmetrical nature of fluid domain. The total length of the test section was six times the channel hydraulic diameter. The rib pitch was ten times the rib height. The ribs were at an angle of attack of 45-degrees with respect to the bulk flow direction. The heat transfer measurement pitch has been identified by red dashed region, which was at a distance of 3.75 times the channel hydraulic

diameter. Although, this length was not sufficient for proper flow development, the smooth converging duct helped in providing a smooth velocity profile at the entrance of the test section.

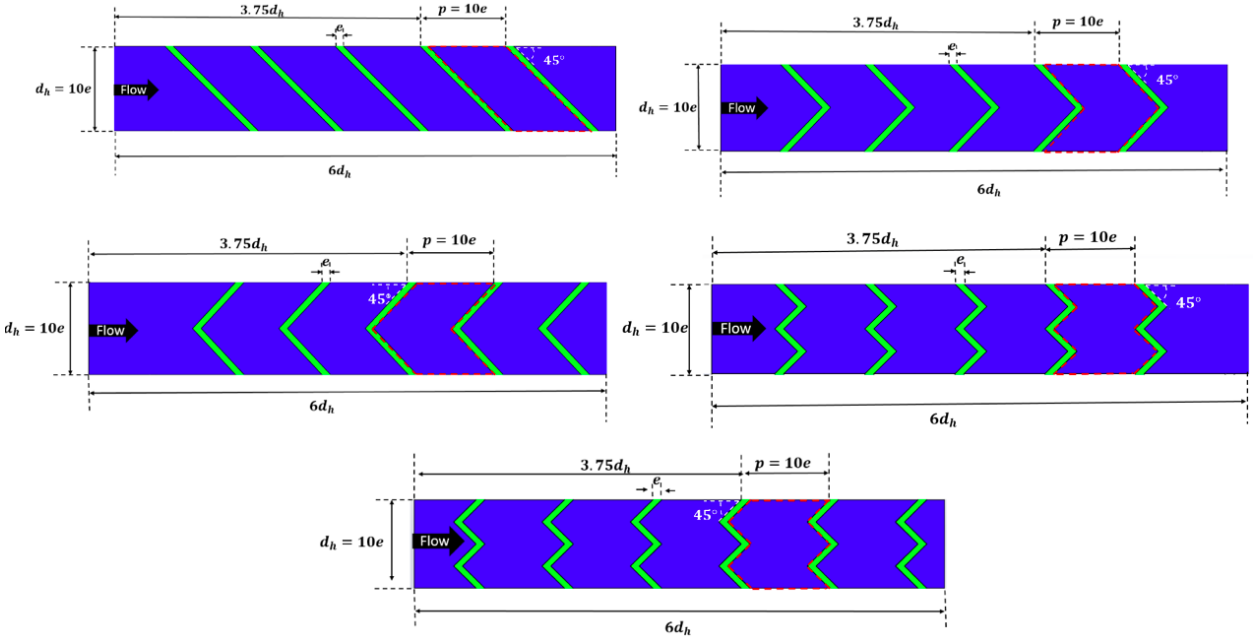

Fig. 3 Test configurations

Steady state liquid crystal thermography experiments were carried out at five Reynolds numbers ranging from 150,000 to 400,000. To calculate normalized friction factor, total pressure drop across the channel was measured.

Reynolds number and Heat transfer coefficient calculation methodology

Reynolds number calculation

The flow Reynolds number was measured by calculation of total mass flow rate flowing through the square duct. Separate experiments were carried out to measure the total mass flow rate at different motor speeds. A pitot tube was sequentially traversed along the channel span at different span wise locations to measure the dynamic pressure head. A total of 15 data points was collected to obtain the velocity profile across the channel span. These measurements were carried out before the flow encountered rib turbulators. Flow velocities were then calculated and were used to calculate the mass flow rate by integrating the velocity profile about the channel span. The dynamic pressure heads measured at different channel span were identical. Also, for the investigated range of Reynolds number, the turbulent boundary layer thickness ranged from 2.8

mm to 3.7 mm, which is negligible in comparison to channel span. Hence, the obtained curve for velocity profile was nearly linear in nature. Reynolds number was then calculated from,

$$Re_{d_h} = \frac{\dot{m}}{\mu d_h} \quad (\boldsymbol{Eq.1})$$

Thermochromic Liquid Crystal (TLC) sheet color change calibration

The liquid crystal thermography technique works on the concept that the different colors can be correlated accurately to known wall temperatures. In this study, we used a Hue-based calibration technique to establish the relationship between Hue and wall temperature. Four T-type thermocouples were taped via. aluminum tape on to the liquid crystal sheet. For calibration experiments, several different heat fluxes were provided to obtain multiple images of LC color change and wall temperatures. The LC color change captured by the CCD camera was transferred to the work station. An in-house code was developed to convert the raw color change to Hue values. Figure 4 shows the variation of Hue with respect to wall temperature. It should be noted that four different thermocouples yielded near-similar calibration curves and the color play was also obtained in the manufacturer specified band. The relationship between wall temperature and Hue will be used later for determination of local wall temperatures. Four identical hue-wall temperature curves indicate that the calibration was high-quality and the subsequent wall temperature calculation through this relationship was very accurate.

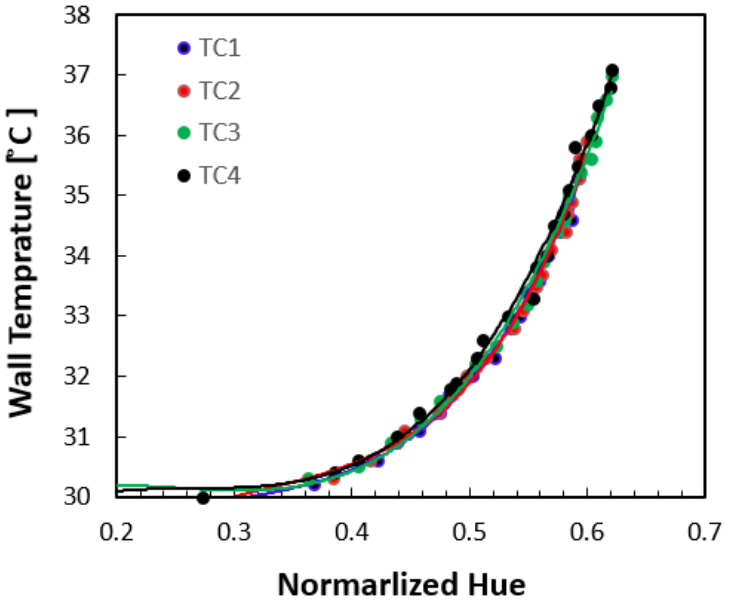

Fig. 4 Wall temperature variation with normalized hue

Heat transfer coefficient calculations

Heat transfer coefficients were calculated by conducting steady-state heat transfer experiments. Although the brass foil was surrounded by insulating materials, there was considerable heat loss which had to be accounted for in the heat transfer coefficient calculations. To that extent, two heat loss experiments were carried out prior to carrying out forced convection experiments. During the heat loss experiments, the duct exit was blocked to avoid any continuous flow of contained air to the laboratory ambient. A constant heat flux was supplied through the heater. However, the steady-state temperatures obtained through liquid crystal color change was not uniform. This was attributed to the presence of channel side walls and rib turbulators which were installed firmly and had good contact with the liquid crystal sheets. Hence, increased losses were found around the side wall edges and rib turbulators through conduction. A local distribution of heat loss was obtained at two different heat flux values. For a given pixel, it was found that the heat loss variation with respect to the difference in the local wall temperature and ambient fluid $(T_w - T_\infty)$ was linear in nature and it is further known that the heat loss was zero when the wall temperature and ambient fluid temperature were same. Based on these three points, a linear relationship was established between heat loss $(q"_{loss})$ and $(T_w - T_\infty)$. Loss coefficient defined by Eq. 2 was then calculated for each pixel in the region of interest.

$$\alpha(x,y) = \frac{q"_{loss}}{(T_w(x,y) - T_\infty)} \quad (\boldsymbol{Eq.2})$$

Samples of loss coefficient contours have been shown for different configurations in Fig. 5. It can be seen that the maximum loss coefficients were found around the edges were conduction losses were dominant compared to natural convection and conduction through surrounding objects having direct contact with brass foil-LC sheet assembly. Further, the LC sheet was assembled such that maximum heat transfer from heater through conduction only, occurred towards the airflow, in order to accurately capture the convective heat transfer rates. The thermal conductivity of brass foil $(109\ W/mK)$ was approximately 570 times higher than the plexiglass $(0.19\ W/mK)$on the backside of the heater. Hence, it can be assumed that the heat losses were only in the direction of ambient air, i.e. the duct where coolant will flow in forced convection experiments.

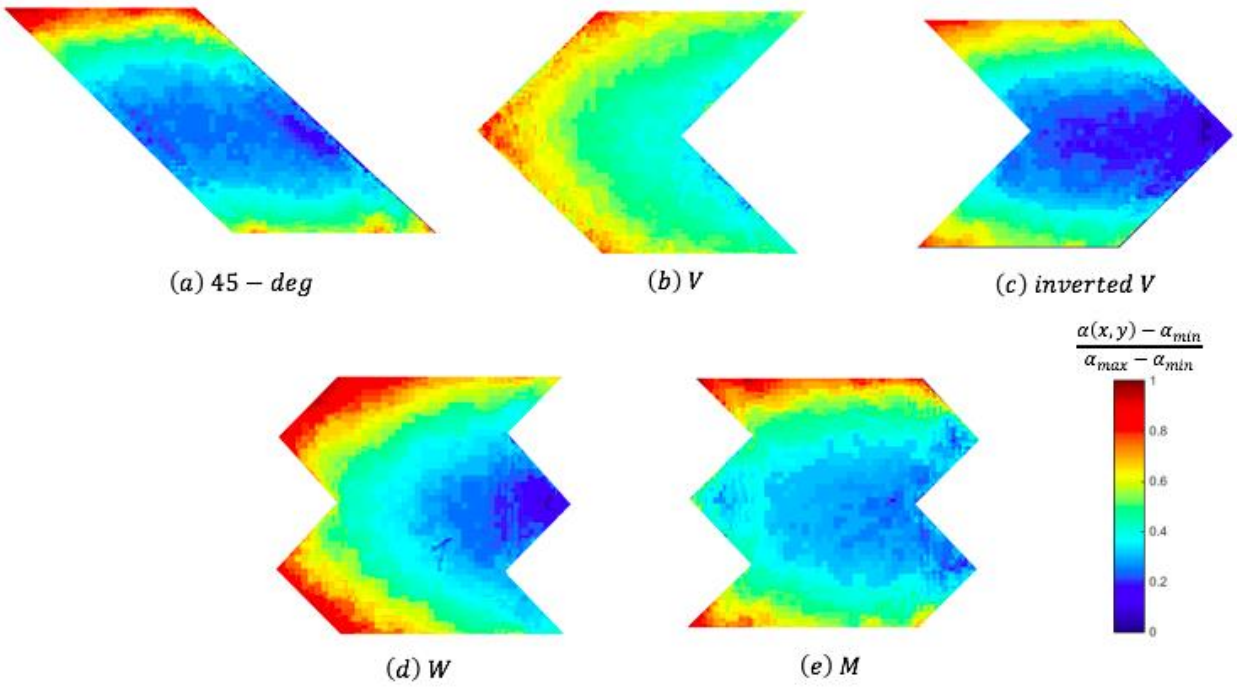

Fig. 5 Normalized loss coefficient (α)

Once the loss coefficient was obtained for each pixel, heat transfer coefficient during forced convection experiments was calculated from,

$$h(x,y) = \frac{\left(q"_{flow} - q"_{loss}(x,y)\right)}{T_w(x,y) - T_\infty(x)} = \frac{\left(q"_{flow} - \alpha(x,y)\left(T_w(x,y) - T_\infty(x)\right)\right)}{T_w(x,y) - T_\infty(x)}$$

$$= \frac{q"_{flow}}{T_w(x,y) - T_\infty(x)} - \alpha(x,y) \quad (\boldsymbol{Eq.3})$$

After a certain Reynolds number was established through the duct, heat flux ($q"_{flow}$) was increased such that every pixel in region of interest had some color change, so that it can be related to a known wall temperature $T_w(x,y)$. The bulk fluid temperatures were measured at the inlet and exit of the test section and also calculated through overall energy balance. Due to addition of heat into the fluid domain, bulk fluid temperature is expected to increase with increasing streamwise distance. However, the total heat addition into the fluid domain was negligible compared to the energy required to raise the fluid temperature by 0.1°C considering very high heat capacity of the fluid flow. Hence, bulk fluid temperature measured at the inlet of the rib pitch where heat transfer coefficient has been calculated, has been used as the reference fluid temperature in Eq. 3.

At steady state, five snapshots were taken and the mean of these five images was used and processed to obtain $T_w(x, y)$. Heat transfer was then calculated using Eq. 3. The normalized Nusselt number was calculated using following equation.

$$\frac{Nu}{Nu_0} = \frac{hd_h}{k_f(0.023{Re_{d_h}}^{0.8}Pr^{0.4})} \quad (\boldsymbol{Eq.4})$$

The thermal conductivity of air was calculated at the film temperature, $T_f = 0.5(T_w + T_\infty)$. The Nusselt number was normalized with Dittus-Boelter correlation for Nusselt number in a developed turbulent flow in circular tube.

UNCERTAINTY ANALYSIS

Present paper reports heat transfer and pressure drop results at different Reynolds numbers. The quantities which have uncertainties are, Reynolds number, friction factor, normalized friction factor, Nusselt number, Nusselt number ratio (Nu/Nu_0) and Thermal Hydraulic Performance. A sequential perturbation method prescribed by Moffat [27] was used for uncertainty calculation. The uncertainty for Reynolds number ranging from 170000 to 370000 varied between 3.7% and 0.68%. The uncertainty in calculation of Nusselt number ratio (Nu/Nu_0) varying between 1.5 and 1.7 was between 10% and 15%. The uncertainty in calculation of normalized friction factor (f/f_0) varying between 8.5 and 10.5 was between 6.5% and 1.5%. The uncertainty in calculation of thermal hydraulic performance varying between 0.65 and 0.8 was between 3.9% and 6.8%.

RESULTS AND DISCUSSION

Detailed Nusselt number ratio (Nu/Nu_0) for different configurations have been presented and discussed in this section. Further, pitch-averaged Nusselt number ratio is presented with respect to Reynolds number. Normalized friction factor and thermal hydraulic performance has been presented with respect to Reynolds number.

Detailed Nusselt number ratio (Nu/Nu_0)

Figure 6 shows the detailed Nusselt number ratio for 45-degree rib configuration. The heat transfer enhancement mechanism by ribs placed at an angle of attack with respect to bulk coolant flow is through formation of thin thermal boundary layer regions and increase in near-wall shear due to combined action of flow re-attachment and increase in near-wall turbulent kinetic energy due to rib induced secondary flows. Further, the rib induced secondary flows interact with duct

sidewalls and result in generation of a counter rotating vortex pair which increases turbulent transport between top and bottom walls subjected to heat loads in actual gas turbine blades. For the case of 45-degree angled rib turbulators, the secondary flows originate from the rib and duct side wall intersection and travels along the rib. The re-attachment of the flow separated due to ribs, results in heat transfer enhancement as a result of very thin thermal boundary layer. Also, the secondary flows enhance the near-wall shear due to a swirling action and increase the near-wall turbulent kinetic energy (TKE).

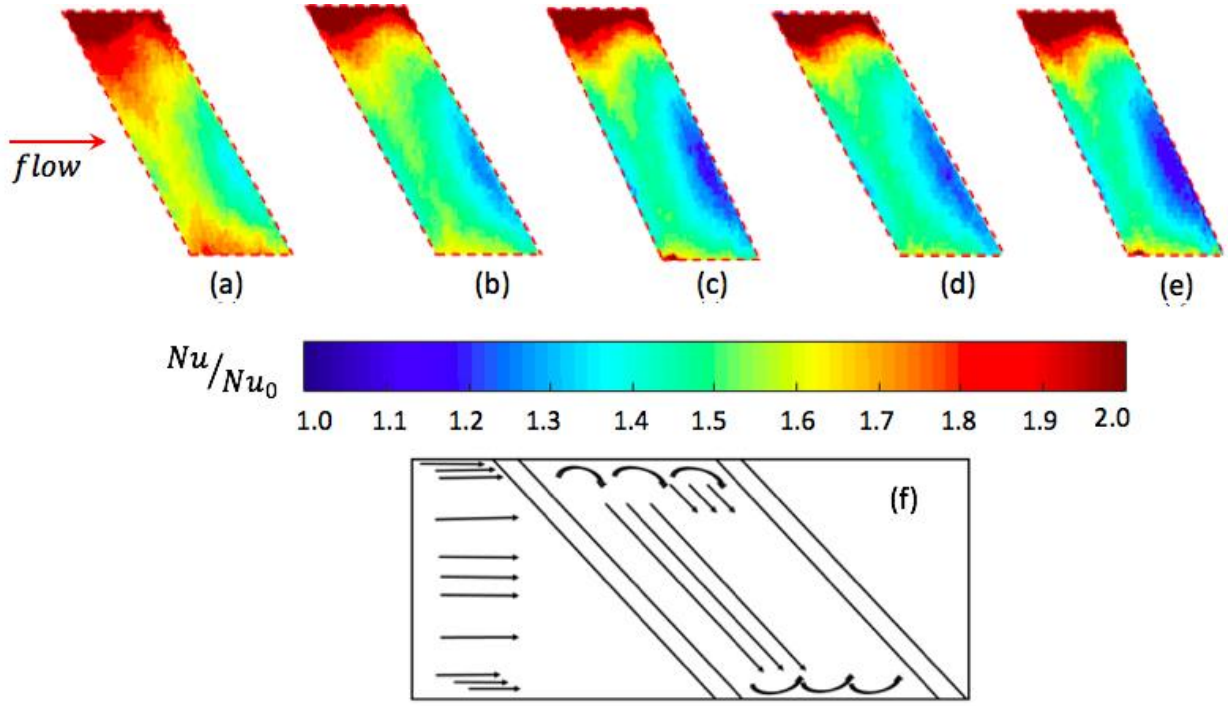

Fig. 6 Nusselt number ratio ($\mathrm{Nu}/\mathrm{Nu}_0$) for 45-deg inclined ribs at selected region $3.75 < x/d_h < 4.75$. (a) Re = 179457, (b) Re = 264199, (c) Re = 307218, (d) Re = 348941, (e) Re = 390986, (f) secondary flow induced by 45-deg inclined ribs.

For very high Reynolds number cases, the Nusselt number ratio levels were nearly similar to each other. In contrast to relatively lower Reynolds number studies on 45-degree angled rib turbulators [12], the higher Reynolds number heat transfer distribution was non-uniform within a rib pitch, with very high heat transfer at one corner and very low heat transfer upstream of the downstream rib. From detailed contours, it is apparent that the flow turning by 45-degree angle of attack was not very effective as has been observed in low Reynolds number studies (up to Reynolds number of 90000) [12]. Further, the deflected flow traveling along the rib, post interaction with the duct sidewall, starts to travel along that wall, resulting in enhanced heat

transfer. A parametric study of the effect of rib angle of attack is recommended for very high Reynolds numbers, as higher angle of attack appears to be more promising in terms of achieving higher heat transfer enhancement.

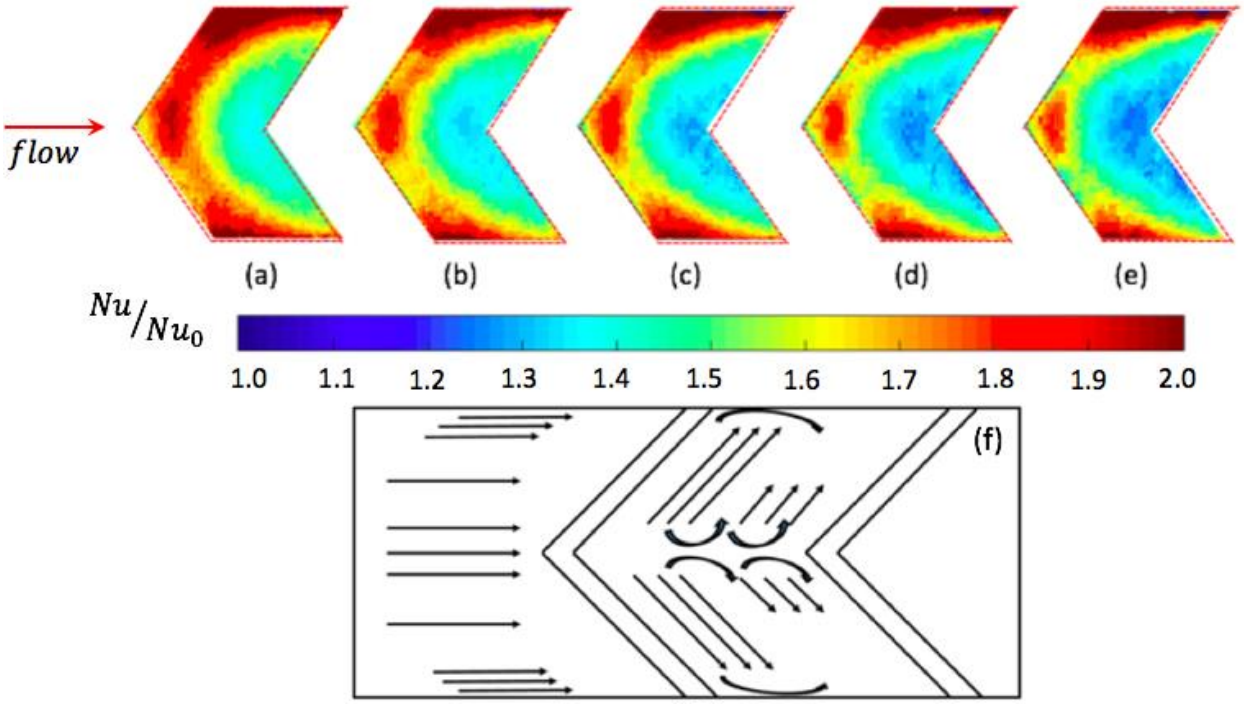

Fig. 7 Nusselt number ratio (Nu/Nu_0) for V-shaped ribs at selected region$3.75 < x/d_h < 4.75$. (a) Re = 168013, (b) Re = 252900, (c) Re = 292468, (d) Re = 334912, (e) Re = 376534, (f) Schematic pattern of the secondary flow induced by V-shaped ribs.

Figure 7 shows the detailed Nusselt number ratio for V-shaped rib turbulators. The heat transfer mechanism for V-shaped ribs is different compared to 45-degree ribs, as there are two 45-degree ribs joined at the channel centerline in V-shape ribs. The coolant interacts with the sharp corner at the channel centerline and secondary flows travel towards duct side wall. Since the ribs were installed on two opposite walls, two pairs of counter-rotating vortices were present in V-shaped configurations, hence the turbulent transport mechanism in V-shaped ribs is stronger compared to 45-degree ribs. The individual strength of turbulent transport of one CRVP will be weaker when compared to the CRVP of 45-degree ribs. Also, the strength of secondary flows induced by V-shaped ribs will be weaker compared to that of 45-degree because of the difference in length of ribs. However, for V-shaped ribs, there are two CRVPs and two secondary flow streams compared to one CRVP and one secondary flow stream in 45-degree ribs. Hence, it is expected that overall heat transfer enhancement of V-shaped ribs will be higher than that of 45-

degree ribs. From detailed contours, it can be seen that the heat transfer enhancement regions were aligned along the ribs. A large region of relatively lower heat transfer enhancement was also seen in V-shaped ribs, again indicating the conventional arrangement of p/e = 10, might be insufficient to allow the expected Nusselt number enhancement contour similar to low Reynolds number cases [12].

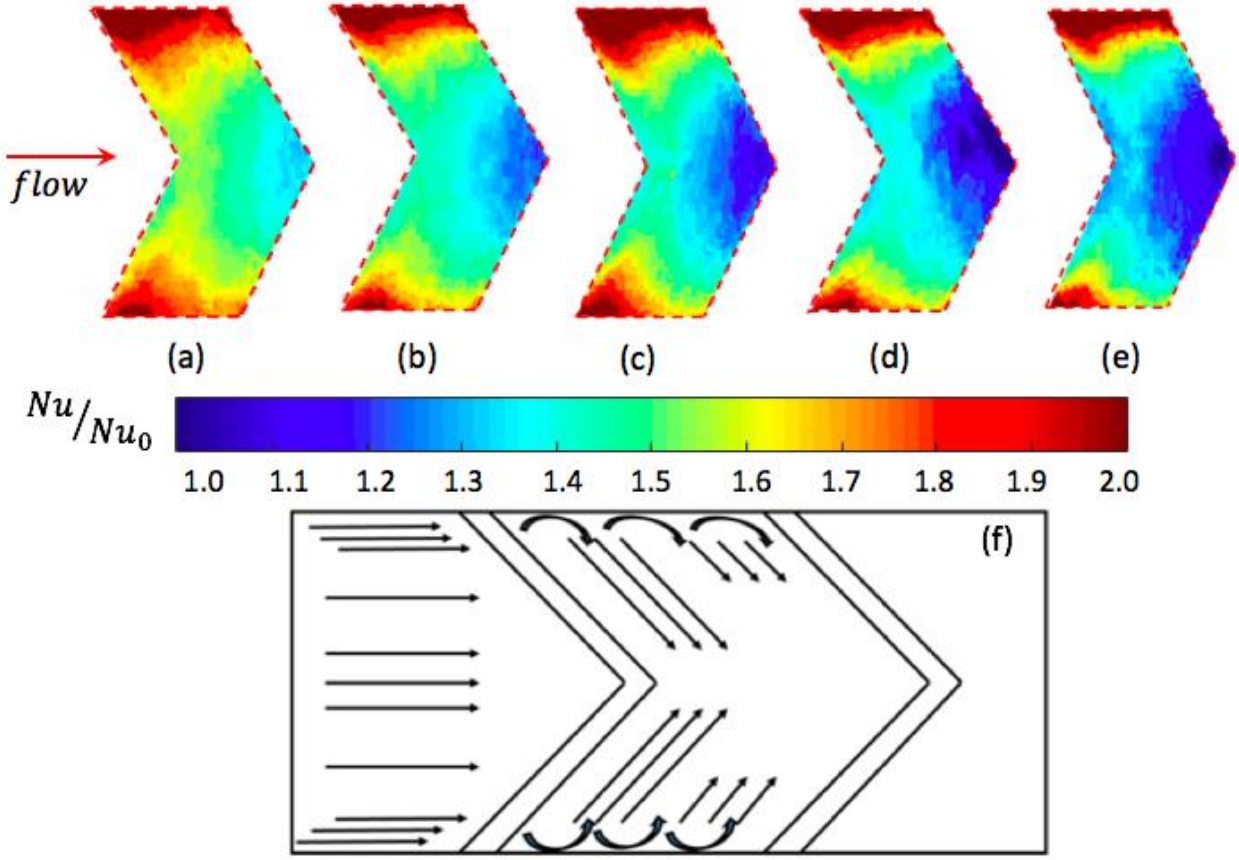

Fig. 8 Nusselt number ratio (Nu/Nu_0) for Inverted V-shaped ribs at selected region $3.75 < x/d_h < 4.75$. (a) Re = 167782, (b) Re = 249689, (c) Re = 291258, (d) Re = 331596, (e) Re = 372244, (f) Schematic pattern of the secondary flow induced by inverted V-shaped ribs.

Figure 8 shows the detailed Nusselt number ratio for the inverse-V shaped ribs. In this case, secondary flows are generated from the corners near the duct side wall and travel towards the channel centerline. Further, two pairs of counter rotating vortices will exist similar to V-shaped ribs. Inverse V-shaped ribs had lower heat transfer compared to the V-shaped ribs. Coolant momentum flux is expected to be higher along the channel centerline, hence the strength of rib induced secondary flows for the V-ribs is expected to be higher compared to the inverse V-

shaped ribs. Low heat transfer regions were observed for inverse-V shaped ribs as well, just upstream of the downstream rib.

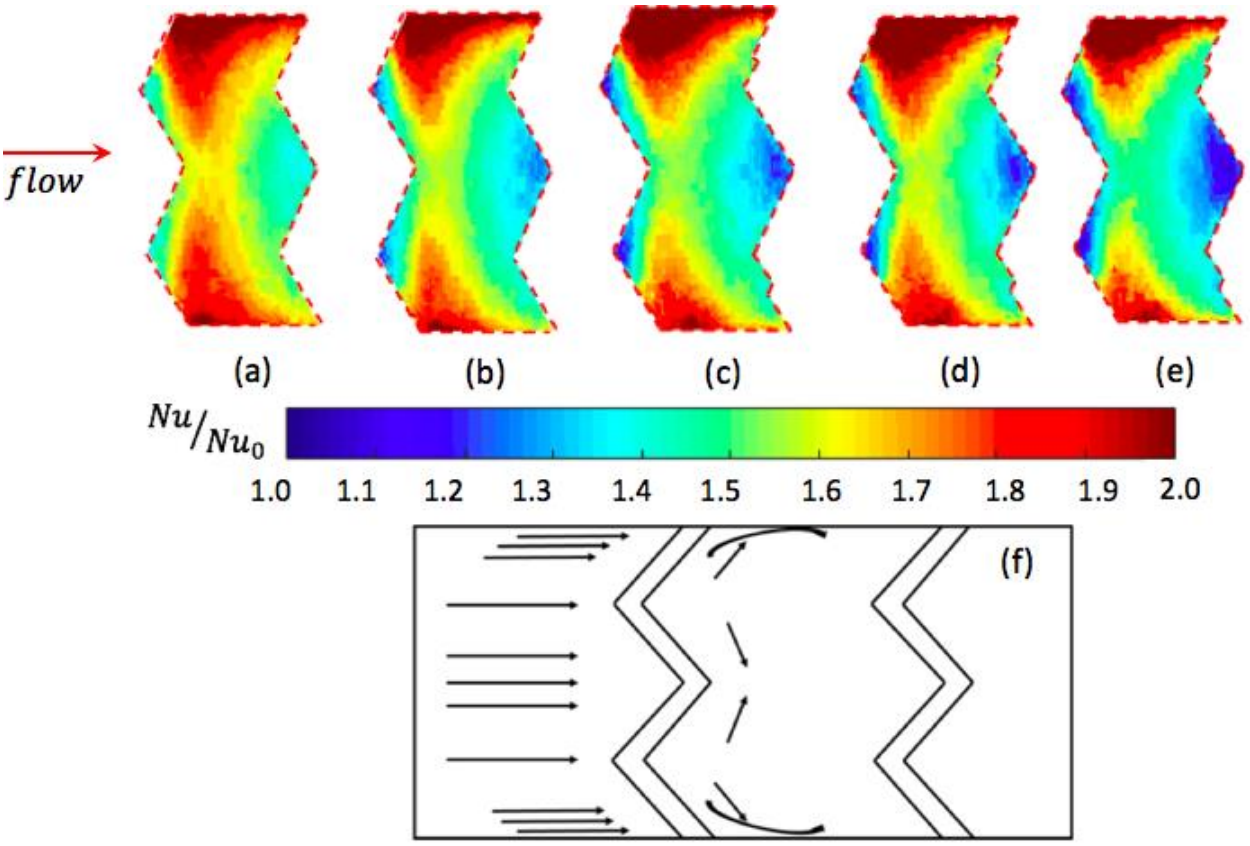

Fig. 9 Nusselt number ratio (Nu/Nu_0) for W-shaped ribs at selected region$3.75 < x/d_h < 4.75$. (a)Re = 169454, (b) Re = 250197, (c) Re = 291584, (d) Re = 331955, (e) Re = 372617, (f) Secondary flow induced by W-shaped ribs.

Figure 9 shows the detailed Nusselt number ratio for W-shaped ribs. The secondary flows originating from the ribs has been shown in Fig. 9 (f). In this case, four pairs of counter rotating vortices are observed due to the presence of two pairs of V-shaped ribs connected at the channel centerline, and installed on two opposite walls. The heat transfer around the duct side wall was found to be higher, since the strength of secondary flows induced from the rib closest to side wall was stronger than those present at channel centerline. Further, due to higher proximity of the rib and side wall, the turbulence transport due to the CRVPs was stronger near the duct side walls. The dominant mechanism for heat transfer in V-shaped and W-shaped ribs is through the turbulence transport due to CRVPs compared to increase in near wall shear due to interaction of secondary flows with the duct end wall.

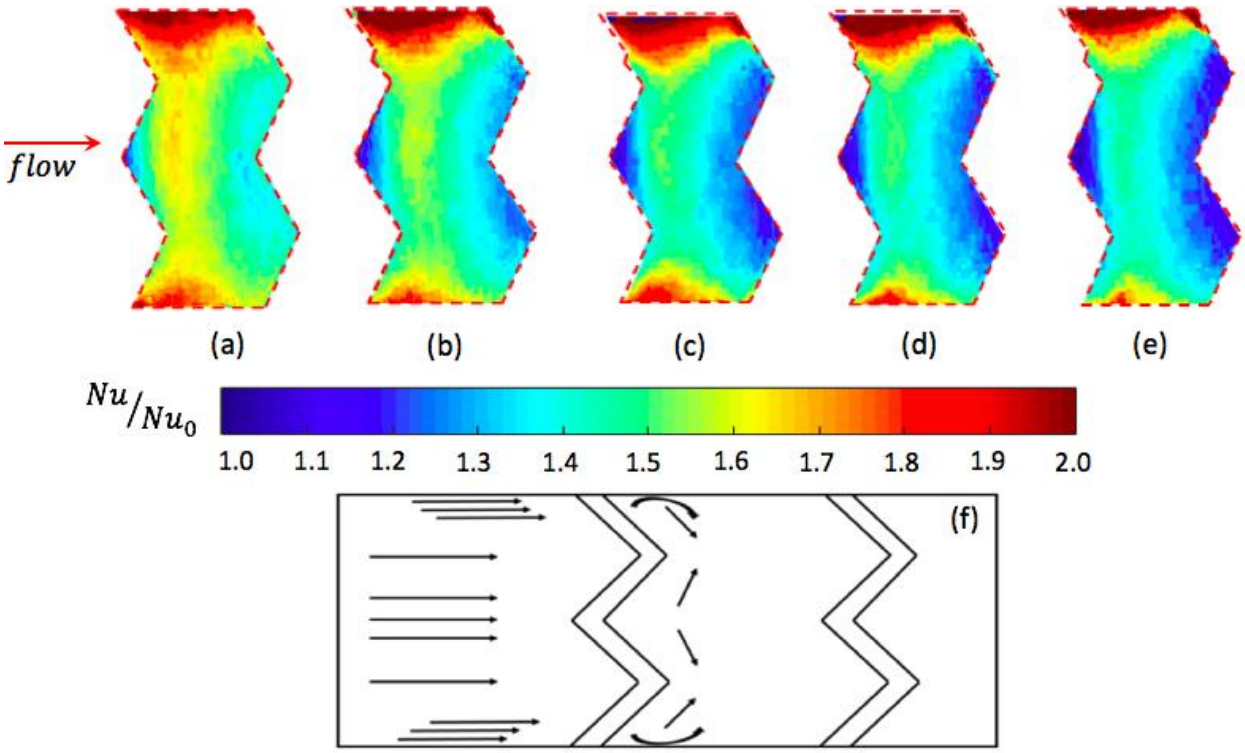

Fig. 10 Nusselt number ratio (Nu/Nu_0) for M-shaped ribs at selected region $3.75 < x/d_h < 4.75$. (a) Re = 169390, (b) Re = 250580, (c) Re = 291744, (d) Re = 332839, (e) Re = 373668, (f) Schematic pattern of the secondary flow induced by M-shaped ribs.

For low Reynolds number cases, the effect of secondary flow induced enhancement in near wall TKE of fluid is the dominant mechanism of heat transfer enhancement, where distinctly symmetric high and low heat transfer regions could be identified [12]. For the inverse-W shaped ribs, referred as M-shaped ribs (Fig. 10), similar trends were observed as was between V-shaped and inverse-V shaped ribs.

Comparing all five configurations in the present study, some generalized comments can be made. 45-degree parallel rib configuration was different from other configurations, since the secondary flows induced travel in only one direction, i.e. along the rib from one side wall to the other. However, V-shaped and W-shaped ribs had some geometrical similarities and inverse-V and M-shaped ribs had some geometrical similarities, in the way how secondary flows propagate within a rib pitch. For V- and W-shaped ribs, the secondary flows induced by the ribs travel towards channel side walls, and this mechanism has been proved to result in enhanced heat transfer because of strengthening of CRVP due to support from channel side wall. Whereas in the

case of inverse-V and M-ribs, the secondary flows originate from the channel side walls and travel towards channel centerline, leading to reduced strength of the CRVPs.

Regionally averaged Nusselt number ratio (Nu/Nu_0), friction factor (f/f_0) and thermal hydraulic performance (THP)

The variation of regionally averaged Nusselt number ratio (Nu/Nu_0) with Reynolds number has been shown in Fig. 11. The rib pitch chosen for averaging the local Nusselt number has been shown in Fig. 3. The enhancement in Nusselt number ratio was found to be decreasing with increasing Reynolds number. This trend has been commonly seen in turbulent flows. With increase in Reynolds number, the near wall turbulent kinetic energy induced by secondary flows by ribs, strengthens. However, this increase in near wall TKE when normalized with square of flow speed (TKE') decreases with increasing Reynolds number. Hence the potential for enhancement in Nusselt number ratio (Nu/Nu_0) reduces. Interestingly, for very high Reynolds numbers, the enhancement levels varied only between 1.4 and 1.7 for all the rib configurations over the entire range of Reynolds number. Also, the dependence of Nusselt number ratio on Reynolds number was found to be weak, in contrast with studies on low Reynolds number range (<90000) [12]. As discussed above, V- and W-shaped ribs had the highest heat transfer followed by 45-degree parallel ribs. For the 45-degree parallel rib case, the strength of rib induced secondary flows (due to longer rib length) balances the reduction in strength in turbulent transport due to less number of counter rotating vortex pair. Inverse-V and M-shaped ribs had lowest heat transfer. M-shaped ribs had the lowest heat transfer because of low strength of rib induced secondary flows and further lower strength of the generated CRVPs.

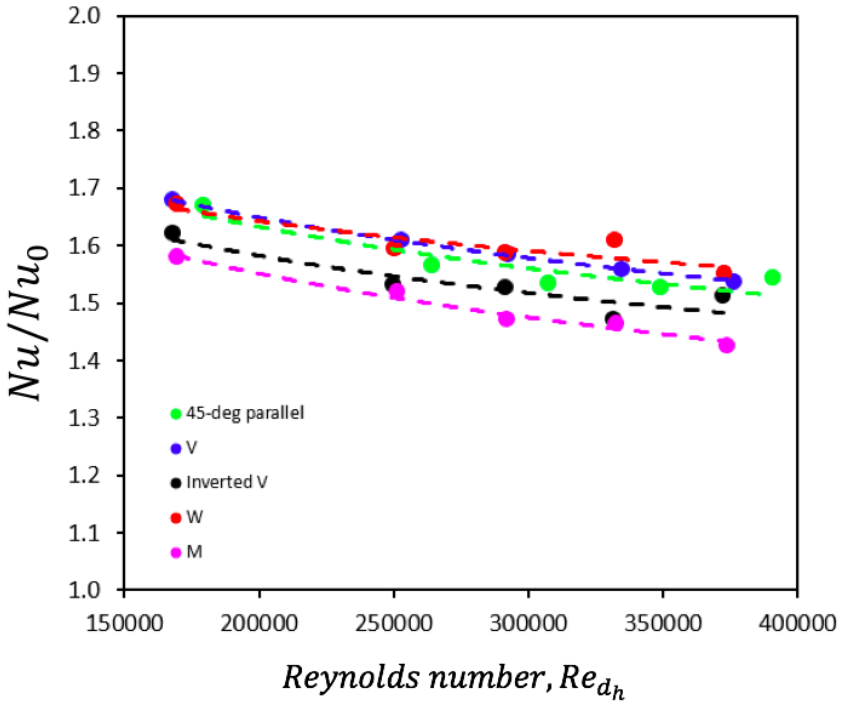

Fig. 11 Regionally averaged Nusselt number ratio variation with Reynolds number

Further, the gain in heat transfer due to rib turbulators result in enhancement in friction factor.

The friction factor comprises of the profile losses due to ribs and geometrical constraints for internal flow in a square channel. In case of turbulent flow over rib turbulators, the profile losses are the major contributors towards the overall friction factor. Friction factor was calculated using the following equation,

$$f = \frac{\Delta p d_h}{2\rho u^2 L} \quad (\boldsymbol{Eq.5})$$

The friction factor was normalized using Swamee-Jain [28] correlation for turbulent flow in circular duct,

$$f_0 = \frac{0.331}{\left(\ln\left(\frac{5.74}{Re^{0.9}}\right)\right)^2} \quad (\boldsymbol{Eq.6})$$

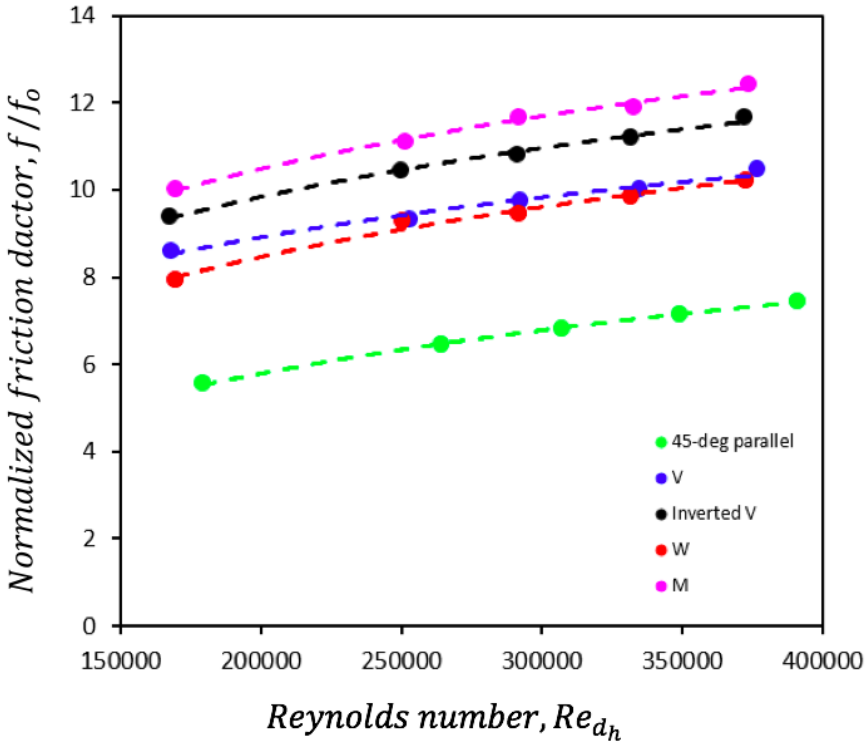

Fig. 12 Normalized friction factor variation with Reynolds number

Figure 12 shows the variation of normalized friction factor with Reynolds number. An increasing trend was observed in friction factor with increasing Reynolds number, which is expected. The 45-degree rib turbulator had the lowest normalized friction factor, and the M-shaped rib had the highest frictional losses.

The thermal hydraulic performance of ribbed channels is given by following equation,

$$THP = \frac{Nu/Nu_0}{(f/f_0)^{1/3}} \quad (\boldsymbol{Eq.7})$$

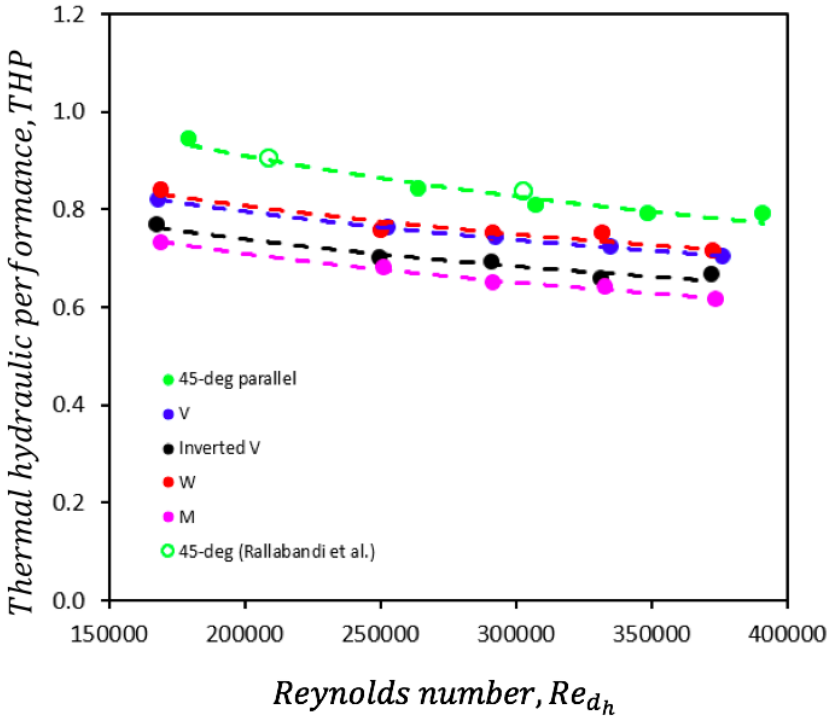

Fig. 13 Thermal Hydraulic Performance variation with Reynolds number

Interestingly, for very high Reynolds number cases, the thermal hydraulic performance for all the investigated rib roughened channels was less than unity, which implies that the rib designs are not effective at elevated Reynolds numbers. Same rib shapes when investigated at Reynolds numbers less than 90000, the thermal hydraulic performance was found to vary between 1.6 and 1.0 with a decreasing trend with increasing Reynolds number [12]. If one has to bridge the thermal hydraulic performance trend between low Reynolds number studies and the present study's high Reynolds number cases, it can be concluded that THP shows an asymptotic trend with increasing Reynolds number with values less than unity at very high Reynolds numbers,

and that the optimized rib turbulator shapes for low Reynolds number are not very effective for high Reynolds number cases. This is an important takeaway from the present study which provides a caution to gas turbine hot gas path designers, particularly for the cases where rib designs for aircrafts are used in land-based power generation gas turbines.

Heat transfer roughness function (G) and friction roughness function (R) variation with Roughness Reynolds number (e+)

Heat transfer roughness function, friction roughness function and roughness Reynolds number has been calculated based on the methodology described in [26]. The equations for G, R and e+ can be found in the nomenclature section. These parameters (G, R and $e^{+)}$ are based on law-of-wall for turbulent flows and are frequently used in generalization of experimental data on different blockage ratio, aspect ratio of channels. Figure 13 shows the variation of friction roughness function with roughness Reynolds number. Friction roughness Reynolds number relates the modified friction factor ($\bar{f} = 2f - f_0$) with channel aspect ratio and blockage ratio. Friction roughness function is inversely proportional to square root of the modified friction factor ($\bar{f}$). As shown in Fig. 12, the normalized friction factor (f/f_0) increased monotonically with increasing Reynolds number. Further, the roughness Reynolds number (e+) is directly proportional to Reynolds number (Re) and modified friction factor. Hence, the variation of R with e^+ was found to have a monotonically decreasing trend with increasing roughness Reynolds number. 45-degree rib turbulators had the lowest frictional losses compared to other rib shapes, and hence the friction roughness function (R) of 45-degree ribs was highest and that of M-ribs was lowest. This parameter R is used in determination of heat transfer roughness function G.

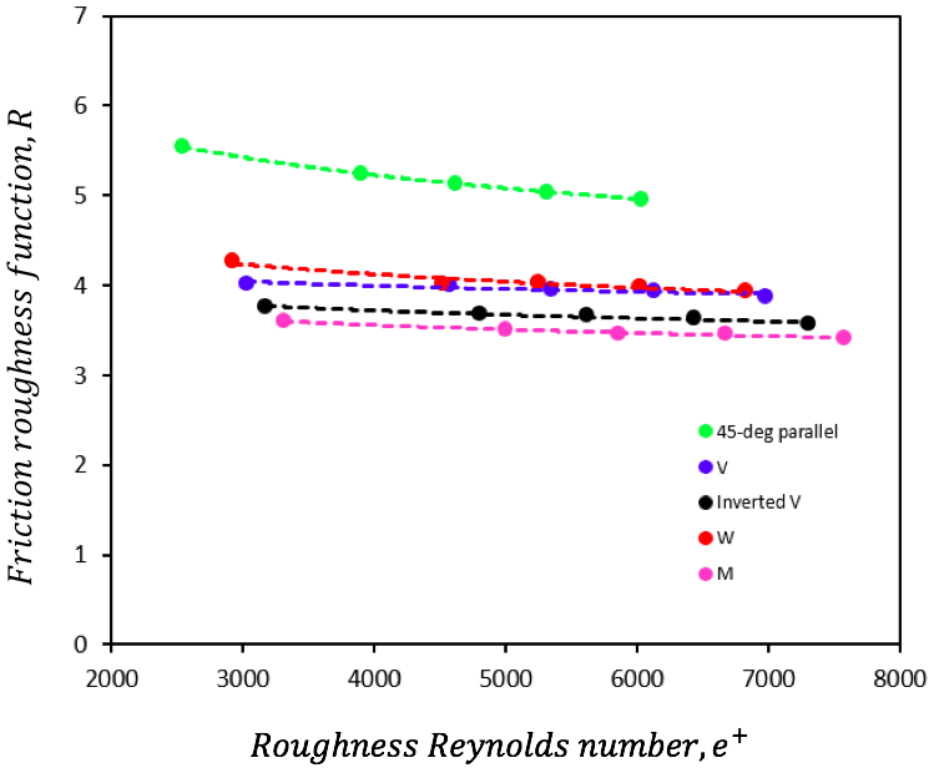

Fig. 14 Friction roughness function (R) variation with roughness Reynolds number (e+)

The heat transfer roughness function (G) combines the heat transfer enhancement with the channel blockage, channel aspect ratio and frictional losses peculiar to rib profiles. Figure 15 shows the variation of Heat transfer roughness function (G) with roughness Reynolds number (e^+). M shaped ribs had the highest heat transfer roughness function and 45-degree ribs were the lowest. Also shown is the comparison with a similar study carried out by Rallabandi et al. [26], and a satisfactory agreement was observed with their high Reynolds number correlation. In an earlier study carried out by Han et al. [29] on various rib shapes for lower Reynolds numbers (<90000), the authors proposed a correlation (Eq. 7) for heat transfer roughness function (G) and roughness Reynolds number (e+).

$$G = 2.24\left(\frac{W}{H}\right)^{0.1}\left(\frac{\alpha}{90°}\right)^{0.35}\left(\frac{p/e}{10}\right)^{0.1}(e^+)^{0.35} \quad (\boldsymbol{Eq.7})$$

Figure 15 shows the G variation with e+ from the correlation prescribed in [29]. It is apparent that the low Reynolds number correlation is not in agreement for high Reynolds number experiments.

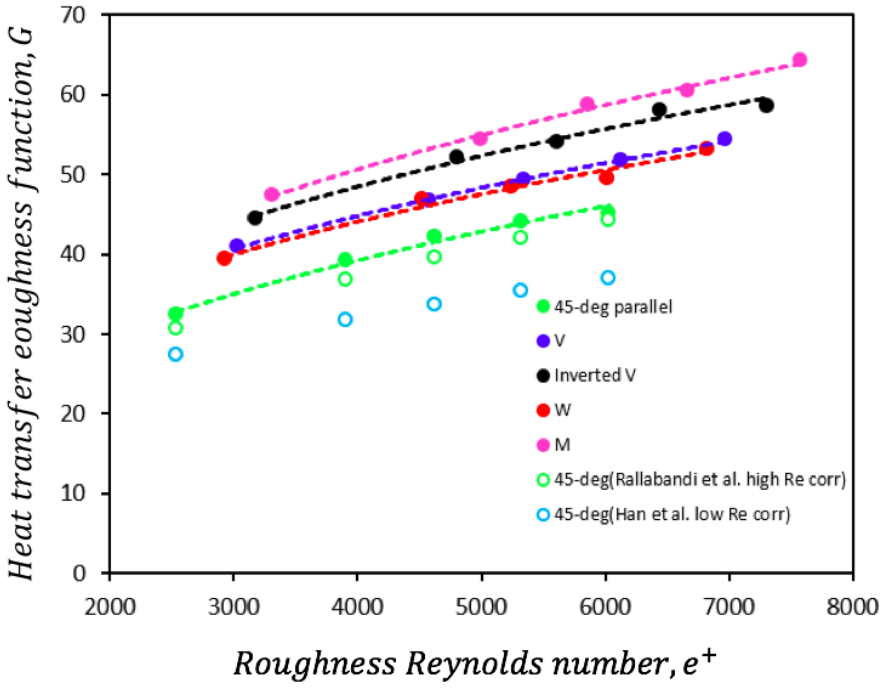

Fig. 15 Heat transfer roughness function (G) variation with roughness Reynolds number (e+)

CONCLUSIONS AND RECOMMENDATIONS

Present study was focused on measurement of detailed heat transfer coefficient at very high Reynolds numbers. A steady-state liquid crystal thermography technique was employed for calculation of heat transfer coefficient. The aim of the study was to evaluate the traditional rib designs at very high Reynolds number, which have been usually investigated for Reynolds numbers less than 90000 in prior studies. For low Reynolds number studies, the optimum parameters ($p/e = 10, e/d_h = 0.1$) defining the rib geometries for high levels of heat transfer, were taken into consideration and heat transfer enhancement levels were evaluated against the increase in frictional losses for Reynolds number ranging between 150000 to 400000. Five different rib configurations, viz. 45-degree, V, inverse-V, W and M shapes have been studied. From the detailed measurements of heat transfer coefficient, it was found that the general trends of heat transfer enhancement for high Reynolds number cases were similar to those observed for low Reynolds number studies, however, some differences were observed in local heat transfer enhancement characteristics. The overall normalized heat transfer coefficient (Nu/Nu_0) showed weak dependence on Reynolds number in the investigated range and varied between 1.4 and 1.7. W-shaped ribs had the highest heat transfer and M-shaped ribs had the lowest heat transfer. The thermal hydraulic performance (THP) was found to be lower than unity for Reynolds numbers

ranging from 150,000 to 400,000. Hence, gas turbine designers should use the optimized geometrical parameters for low range Reynolds number, in land-based power generation gas turbines with caution. Additionally, a parametric study is recommended to obtain optimized geometrical parameters defining rib roughened ducts for Reynolds numbers ranging between 10^5 and 10^6.

NOMENCLATURE

d_h	channel hydraulic diameter
e	rib height
e^+	roughness Reynolds number, $(e/D)Re\sqrt{0.5\bar{f}}$
f	friction factor
$\bar{f}$	modified friction factor, $f + (H/W)(f - f_0)$
f_0	friction factor from modified Blasius correlation
G	heat transfer roughness function, $R + \left(\left(0.5\,\bar{f}/St\right) - 1\right)/\left(\sqrt{0.5\bar{f}}\right)$
h	heat transfer coefficient
H	height of the channel
k_{air}	thermal conductivity of air
L	length of the test section
Nu	local Nusselt number
Nu_0	Nusselt number (D-B correlation)
p	rib pitch
Δp	pressure drop across test section
p_t	stagnation pressure

p_s static pressure

R Friction roughness function, $\sqrt{2/\bar{f}} + 2.5ln\left(4eW/\left(D(W+H)\right)\right) + 2.5$

Re Reynolds number

St Stanton number, $Nu/(RePr)$

T_w wall temperature

T_b bulk temperature

q_{loss} heat loss on the wall

V voltage supplied by power source

A area of heated surface

R resistance of flexible heater

THP thermal hydraulic performance

u average coolant velocity in the duct

W width of the channel

Greek symbols

α heat loss coefficient

ρ density of air

μ viscosity of air

REFERENCE

1. Han J. C., Dutta S., and Ekkad S., 2012, Gas turbine heat transfer and cooling technology, CRC Press, Boca Raton, Florida, USA.
2. Han J. C., Glicksman L. R., Rohsenow W. M., 1978, "An investigation of heat transfer and friction for rib-roughened surfaces" Int. J. Heat Mass Transf. Vol. 21, pp. 1143-1156.
3. Kiml R., Mochizuki S., and Murata A., 2001, "Effects of Rib Arrangements on Heat Transfer and Flow Behavior in a Rectangular Rib-Roughened Passage: Application to Cooling of Gas Turbine Blade Trailing Edge," ASME J. Heat Transfer, 123, pp. 675–681.

4. Casarsa L., Cakan M., and Arts T., 2002, “Characterization of the Velocity and Heat Transfer Fields in an Internal Cooling Channel with High Blockage Ratio,” ASME Paper No. GT-2002-30207.
5. Rau G., Çakan M., Moeller D., and Arts T., 1998, “The Effect of Periodic Ribs on Local Aerodynamic and Heat Transfer Performance of a Straight Cooling Channel,” ASME J. Turbomach., 120_2_, pp. 368–375.
6. Han J. C., 1984, “Heat Transfer and Friction in Channels with Two opposite Rib-Roughened Wails” ASME J. Heat Transfer. Vol. 106, pp 774-781.
7. Han J. C., Huang J. J., and Lee C. P., 1993, “Augmented Heat Transfer in Square Channels With Wedge-Shaped and Delta-Shaped Turbulence Promoters,” J. Enhanced Heat Transfer, v1.i1.40, pp. 37–52.
8. Lau, S.C., Kukreja, R.T. and McMillin, R.D., 1991. Effects of V-shaped rib arrays on turbulent heat transfer and friction of fully developed flow in a square channel. *International Journal of Heat and mass transfer*, *34*(7), pp.1605-1616.
9. Jia R. G., Saidi A., and Aundwn B., 2002, “Heat transfer enhancement in square ducts with V-shaped ribs of various angles” ASME Turbo., pp. 469-476.
10. Singh, P., Ji, Y., Zhang, M. and Ekkad, S.V., 2017, July. Heat Transfer Enhancement by Criss-Cross Pattern Formed by 45° Angled Rib Turbulators in a Straight Square Duct. In ASME 2017 Heat Transfer Summer Conference (pp. V001T06A003-V001T06A003). American Society of Mechanical Engineers.
11. Singh, P., Pandit, J. and Ekkad, S.V., 2017, “Characterization of heat transfer enhancement and frictional losses in a two-pass square duct featuring unique combinations of rib turbulators and cylindrical dimples” International Journal of Heat and Mass Transfer, 106, pp.629-647.
12. Singh, P., Ravi, B. V., and Ekkad, S., 2016, “Experimental and numerical study of heat transfer due to developing flow in a two pass rib roughened square duct” Int. J. Heat and Mass Transfer, 102, pp. 1245-1256.
13. Singh, P., and Ekkad, S., 2016, June. “Effects of Rotation on Heat Transfer due to Jet Impingement on Cylindrical Dimpled Target Surface” In ASME Turbo Expo 2016:

Turbomachinery Technical Conference and Exposition (pp. V05BT16A010-V05BT16A010). American Society of Mechanical Engineers.

14. Singh, P., and Ekkad, S.V., 2017, ”Effects of spent air removal scheme on internal-side heat transfer in an impingement-effusion system at low jet-to-target plate spacing” International Journal of Heat and Mass Transfer, 108, pp.998-1010.
15. Singh, P., and Ekkad, S., 2017, “Experimental Study of Heat Transfer Augmentation in a Two-pass Channel Featuring V-shaped Ribs and Cylindrical Dimples” Applied Thermal Engineering, 116C, pp. 205-216.
16. Leiss C., 1975, “Experimental investigation of film cooling with injection from s row of holes for the application to gas turbine blades” ASME J. Engineering for Power, 97, pp 21-27.
17. Han J. C., Zhang L., and Ou S., 1993, “Influence of unsteady wake on the heat transfer coefficients from a gas turbine blades” ASME J. Heat Transfer, 115, pp 904-911.
18. Han J. C., 1988, “Heat Transfer and Friction Characteristics in Rectangular Channels with Rib Tabulators” J. Heat Transfer, Vol. 110, pp 321-328.
19. Fan C. S., and Metzger D. E., 1987, “Effect of channel aspect ratio on heat transfer in rectangular passage sharp 180-deg turns” ASME Paper 87-GT-113.
20. Wagner J. H., Johnson B. V., and Hajek T. J., 1991, “Heat transfer in rotating passaged with smooth walls and radial outwards flow” ASME Journal of Turbomachinery, 113, pp 42-51.
21. Han J. C., Zhang P., Lee C. P., 1992, “Influence of surface heat flux ratio on heat transfer augmentation in square channels with parallel, crossed, and V-shaped angled ribs” ASME Journal of Turbomachinery, 114, pp 872-880.
22. Ekkad, S. V, and Han, J. C., 1997, “Detailed heat transfer distributions in two-pass square channels with rib turbulators,” Int. J. Heat Mass Transfer, 40(11), pp. 2525–2537.
23. Jenkins, S. C., Zehnder, F., Shevchuk, I. V., von Wolfersdorf, J., Weigand, B., and Schnieder, M., 2013, “The Effects of Ribs and Tip Wall Distance on Heat Transfer for a Varying Aspect Ratio Two-Pass Ribbed Internal Cooling Channel,” J. Turbomach., 135(2), pp. 021001-1-021001-9.
24. Tanda, G., and Abram, R., 2009, “Forced convection heat transfer in channels with rib turbulators inclined at 45 deg”, Journal of Turbomachinery, 131(2), 021012.

25. Tanda, G., 2011, “Effect of rib spacing on heat transfer and friction in a rectangular channel with 45 angled rib turbulators on one/two walls”, Int. J. Heat and Mass Transfer, 54(5), 1081-1090.
26. Rallabandi, A.P., Yang, H. and Han, J.C., 2009, “Heat transfer and pressure drop correlations for square channels with 45 deg ribs at high Reynolds numbers” Journal of Heat Transfer, 131(7), pp.071703.
27. Moffat, R.J., 1985, “Using uncertainty analysis in the planning of an experiment” ASME, Transactions, Journal of Fluids Engineering (ISSN 0098-2202), 107, pp.173-178.
28. Swamee, P. K., Jain, A. K., 1976, “Explicit equations for pipe flow problems” Journal of the Hydraulics Division, 102(5), pp. 657-664.
29. Han, J.C. and Park, J.S., 1988. Developing heat transfer in rectangular channels with rib turbulators. International Journal of Heat and Mass Transfer, 31(1), pp.183-195.